

# Supplementary Material

## Abstract

*In the supplementary material, we discuss the kernel segmentation of the PSFs that were estimated from the images in our dataset. The estimated depth maps for the real experiments are shown. We also compare the results from our method with those from the single image deblurring techniques of [10] and [23].*

## 1. Blur kernels and depth maps of the results

We initially discuss the kernel segmentation process for our first synthetic experiment (Fig. 1 of the submitted manuscript). The patches used for blur kernel estimation are marked in the observations in Figs. 1 (a) and (b). On the set of blur kernels corresponding to one of the observations (denoted by  $h_1^1, h_1^2, \dots, h_1^6$ ), we applied the kernel segmentation procedure to obtain PSFs from a single depth layer. For every blur kernel  $h_1^c$ , we obtained its support  $\Lambda_1^c$ . The transformation space was defined as follows:  $\theta$  varied between  $-1.6$  degrees and  $1.6$  degrees in steps of  $0.2$  degrees, and  $t_x$  and  $t_y$  ranged between  $-11$  and  $11$  in steps of one pixel. In an estimate of a blur kernel, there can be errors of small magnitudes. Therefore, we consider that the value of a blur kernel at a location is positive only when it is greater than a threshold  $\delta_{th}$ . Consequently, the support is defined as  $\Lambda_1^c = \{\lambda : h_1^c(i, j; i_\lambda - i, j_\lambda - j) > \delta_{th}\}$ . The value of  $\delta_{th}$  was chosen to be  $0.015$ . The support of the estimated blur kernel  $h_1^6$ , denoted by  $\Lambda_1^6$  is depicted in Fig. 2. Each plot in Fig. 2 indicates the set of valid translations corresponding to an angle in the transformation space. The true TSF will contain only a small fraction of the transformations in  $\Lambda_1^6$ .

The second row of Fig. 1, shows the true blur kernels (generated from the known TSF according to the depth values) at the centers of the patches of the two observations on a grid of size  $23 \times 23$ . The locally estimated PSFs were close to the true blur kernels. The first six blur kernels of the second row of Fig. 1 correspond to the true values of  $h_1^1, h_1^2, \dots, h_1^6$ . For every pair of blur kernels, we compared the support of one of the blur kernel with the support of the shifted version of the other and verified whether the two kernels are from the same depth. We illustrate the kernel segmentation process on two pairs of blur kernels. For com-

paring  $h_1^2$  and  $h_1^6$ , the intersection of their supports  $\Lambda_1^{26}$  was determined. Two sets of displacements obtained by applying the transformations of  $\Lambda_1^{26}$  on the points  $\mathbf{p}_2$  and  $\mathbf{p}_6$ , are shown in Figs. 1 (e) and (g), respectively. The locations of positive values of the estimated blur kernels  $h_1^2$  and  $h_1^6$  are shown in Figs. 1 (d) and (f), respectively. From Figs. 1 (d) and (e), we can see that the set of displacements (Fig. 1 (e)) does not fully include the locations of the positive values of the estimated blur kernel (Fig. 1 (d)). Similarly, for the kernel  $h_1^6$ , the set of displacements (Fig. 1 (g)) does not contain all the locations of the positive values of the estimated blur kernel (Fig. 1 (f)). This was observed for any shifted version of  $h_1^6$ . Hence, as per our discussion in section 4.1.1 of the paper, we can infer that  $h_1^2$  and  $h_1^6$  are not from the same depth layer. When we compared  $h_1^3$  and  $h_1^6$ , for a particular shift, the set of displacements of  $\mathbf{p}_2$  and  $\mathbf{p}_6$  were obtained as shown in Figs. 1 (i) and (k). The locations of positive values of  $h_1^3$  and  $h_1^6$  are shown in Figs. 1 (h) and (j), respectively. For this pair of blur kernels, we see that the location of the positive values are within the set of displacements (Figs. 1 (i) and (k)). Therefore, the kernels,  $h_1^3$  and  $h_1^6$  are from the same depth. Using our scheme, we were able to deduce that  $h_1^1$  and  $h_1^2$  are from one depth layer and  $h_1^3, h_1^4, h_1^5$ , and  $h_1^6$  are from the other layer (which was chosen as the reference).

From  $h_1^3, h_1^4, h_1^5$  and  $h_1^6$ , we estimated the TSF after the kernel alignment step. Similarly, the TSF of the second observation was determined. The results of the kernel segmentation and alignment of the first observation are valid even for the second observation. To verify our estimates of the TSFs, we generated blur kernels at the centers of image patches as shown in the third row of Fig. 1. In the second and third rows of Fig. 1, we observe that except for  $h_1^1$  and  $h_1^2$ , the blur kernels obtained from the estimated TSF match closely with the true blur kernels. Since  $\mathbf{p}_1$  and  $\mathbf{p}_2$  were at the foreground, the extent of the true blur kernels  $h_1^1$  and  $h_1^2$  is much larger than the kernels generated from the reference TSF (which was estimated for the background). This also demonstrates the fact that the effective transformations are different for different depths. We also observe a small shift between the estimated and the true kernels because, the optimal shifts determined by the kernel alignment step need not be equal to the original shifts.

Figs. 3 (a) and (b) show the patches used for kernel es-

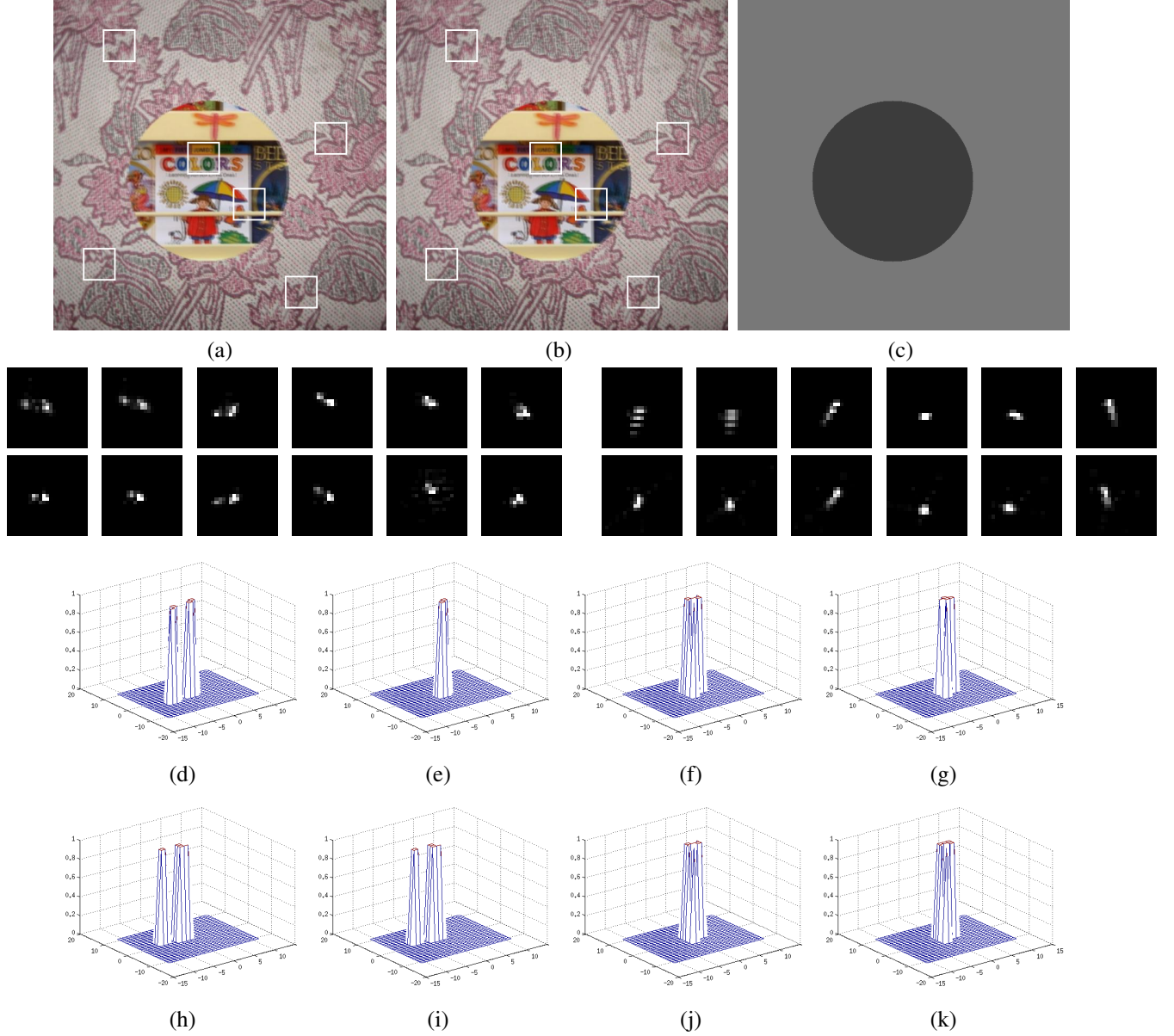


Figure 1. (a) and (b) Blurred observations. (c) True depth map. Second row: True blur kernels (according to the depth map) of the two observations. Third row: Blur kernels generated from the estimated TSF. (d) and (f) locations of the positive values of  $h_1^2$  and  $h_1^6$ . (e) and (g) set of displacements of  $\mathbf{p}_2$  and  $\mathbf{p}_6$  obtained from  $\Lambda_1^{26}$ . (h) and (j) locations of the positive values of  $h_1^3$  and  $h_1^6$ . (i) and (k) set of displacements of  $\mathbf{p}_3$  and  $\mathbf{p}_6$  obtained from  $\Lambda_1^{36}$ .

timination in our first real experiment (first row of Fig. (2) of the manuscript). The blur kernels determined from these patches are shown in the second row of Fig. 3, wherein the first seven blur kernels ( $h_1^1 h_1^2 \dots h_1^7$ ) correspond to the first observation and the remaining seven ( $h_2^1 h_2^2 \dots h_2^7$ ) are from the second observation. The locations of positive values of  $h_1^2$  and  $h_1^7$  are shown in Figs. 3 (c) and (e), respectively. For this pair of blur kernels, the set of displacements of  $\mathbf{p}_2$  and  $\mathbf{p}_7$  obtained from  $\Lambda_1^{27}$  are shown in Figs. 3 (d)

and (f), respectively. In these plots, we observe that the sets of displacements do not include all the locations of the positive values of the blur kernels. Hence, the points  $\mathbf{p}_2$  and  $\mathbf{p}_7$  have different depth values. In contrast, when the supports of  $h_1^1$  and  $h_1^2$  were compared, we found that the points  $\mathbf{p}_1$  and  $\mathbf{p}_2$  are from the same depth layer. This can be inferred from the plots in Figs. 3 (g), (h), (i), and (j). Based on our segmentation process, it was inferred that the points  $\mathbf{p}_1$ ,  $\mathbf{p}_2$ ,  $\mathbf{p}_3$ , and  $\mathbf{p}_4$  were from the same depth layer

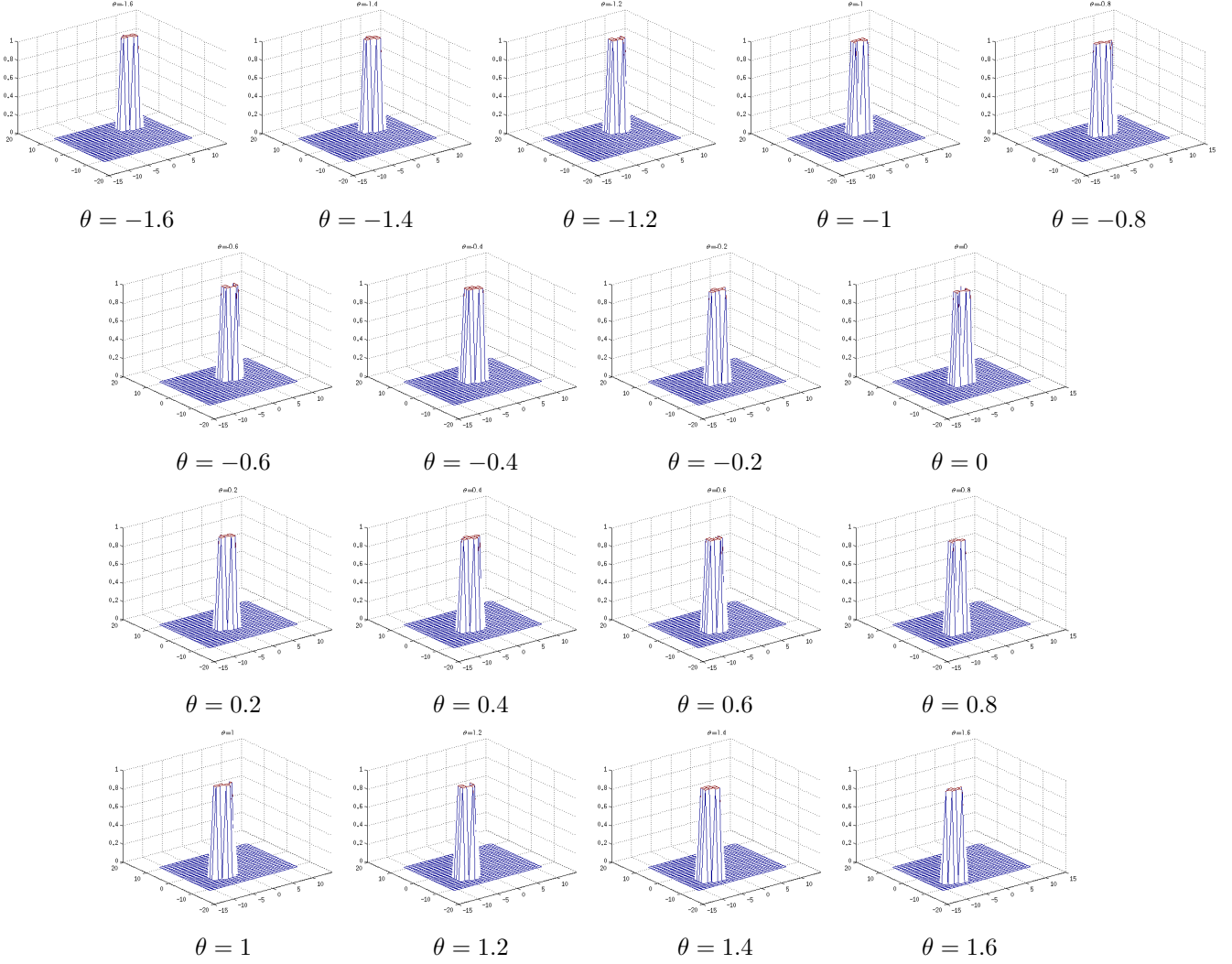


Figure 2. Support of  $h_1^6$ .

(which was regarded as the reference). The TSFs of the two observations were estimated using blur kernels from the reference depth layer. The blur kernels generated from the estimated TSFs are shown in the third row of Fig. 3, wherein we observe that at the points  $\mathbf{p}_1$ ,  $\mathbf{p}_2$ ,  $\mathbf{p}_3$ , and  $\mathbf{p}_4$ , the blur kernels generated from the estimated TSFs match the observed blur kernels (second row). In contrast, since the points  $\mathbf{p}_5$ ,  $\mathbf{p}_6$  and  $\mathbf{p}_7$  are from the background, the blur kernels generated from the reference TSF (at the foreground) do not match the observed blur kernels. From the TSFs and the observations, the depth map was obtained as shown in Fig. 3 (k), and was segmented to two layers (Fig. 3 (l)).

For our second real experiment (third row of Fig. 2 in the manuscript), the local PSFs were estimated using six patches from the two blurred observations as shown in Fig.

4 (a) and (b). The local PSFs are shown in the second row of Fig. 4. We applied our kernel segmentation procedure on the blur kernels from the first observation and found that the first four blur kernels belong to the same layer. We estimated the TSFs from the first four blur kernels of the two observations. The PSFs generated from the estimated TSFs are shown in the third row of Fig. 4. From the second and third rows of Fig. 4, we see that the blur kernels generated from the estimate TSFs match the observed blur kernels only for the first four points. Since the other two points were closer to the camera, we observe that the extent of the observed blur kernels for those points is larger than the blur kernels that were generated from the TSF. From the two TSFs and the observations, we arrived at the depth map as shown in Fig. 4 (c). The depth map was segmented to obtain two depth layers as shown in Fig. 4 (d).

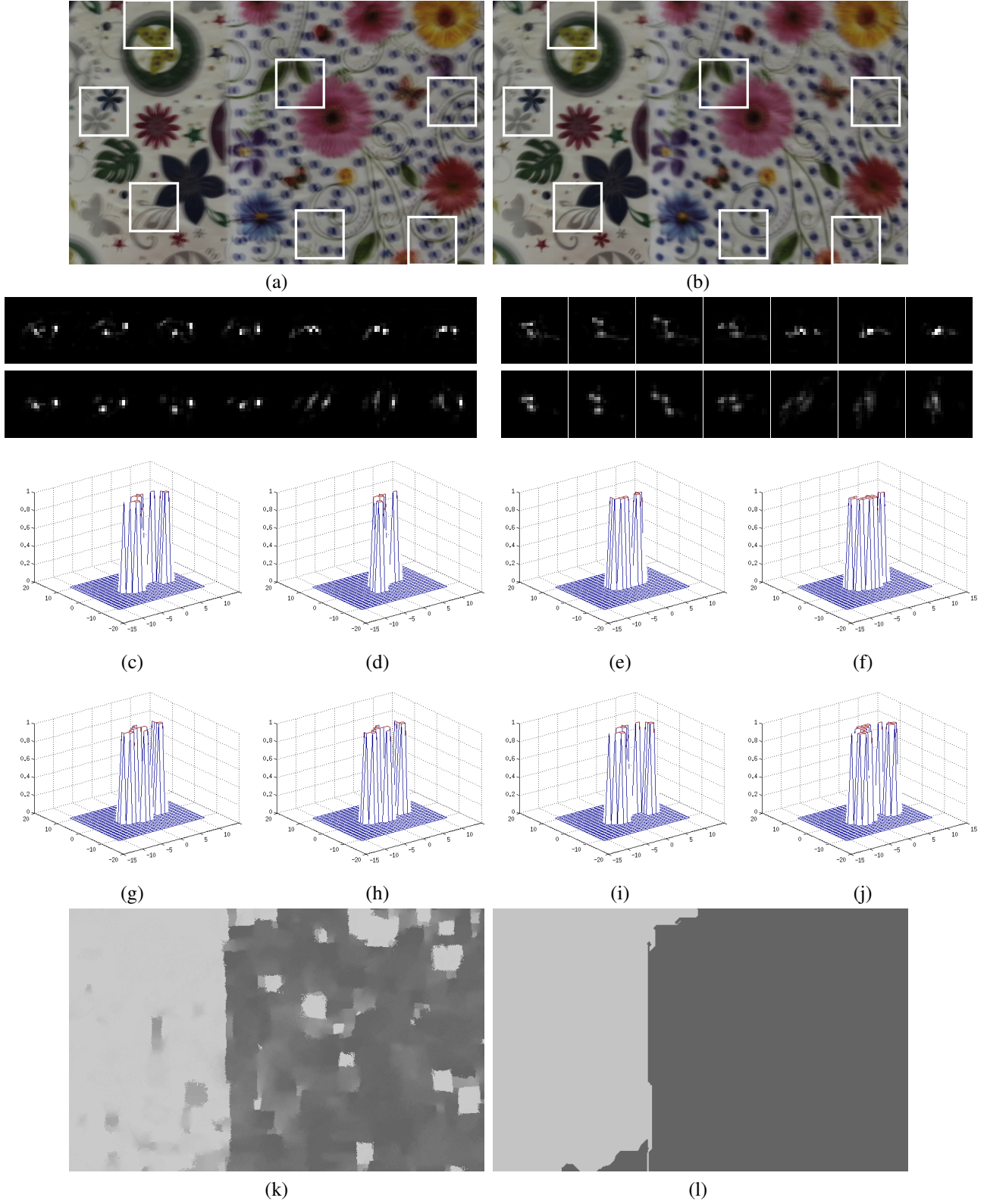


Figure 3. (a) and (b) Blurred observations. Second row: locally estimated blur kernels. Third row: blur kernels generated from the estimated TSFs (of the two observations). (c) and (e) locations of the positive values of  $h_1^2$  and  $h_1^7$ , respectively. (d) and (f) set of displacements of  $\mathbf{p}_2$  and  $\mathbf{p}_7$  obtained from  $\Lambda_1^{27}$ . (g) and (i) locations of the positive values of  $h_1^1$  and  $h_1^2$ . (h) and (j) set of displacements of  $\mathbf{p}_1$  and  $\mathbf{p}_2$  obtained from  $\Lambda_1^{12}$ . (k) Estimated depth map. (l) Segmented depth map.



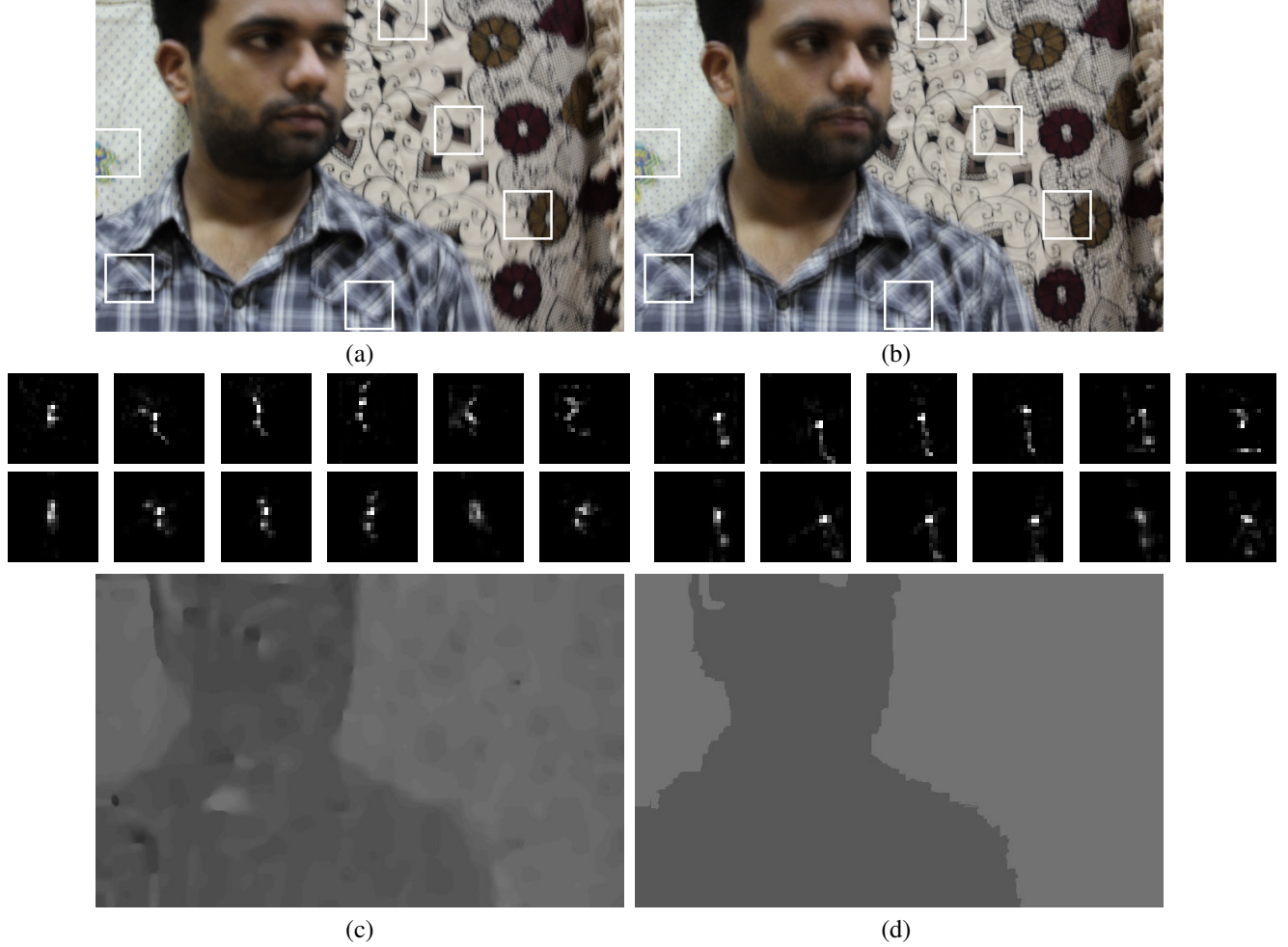


Figure 4. (a) and (b) Blurred observations. Second row: locally estimated blur kernels. Third row: blur kernels generated from the estimated TSFs (of the two observations). (c) Estimated depth map. (d) Segmented depth map.

## 2. Comparisons

For the purpose of comparison, we applied the blind deblurring algorithms of [10] and [23] on images of our dataset. Since [10] and [23] use a single blurred image, only one of the two blurred observations was fed as the input. While the comparisons for the synthetic example are shown in Fig. 5, those for the real experiments are shown in Fig. 6. In Figs. 5 and 6, we observe that the results from our method are much superior to those from the techniques in [10] and [23]. It must be noted that the techniques in [10] and [23] do not account for depth variations both in the blur estimation step as well in restoration. Although this is not a fair comparison (since our method used two observations), the results indicate that the bilayer scene deblurring problem is quite challenging and the current state-of-the-art methods are not adequate.

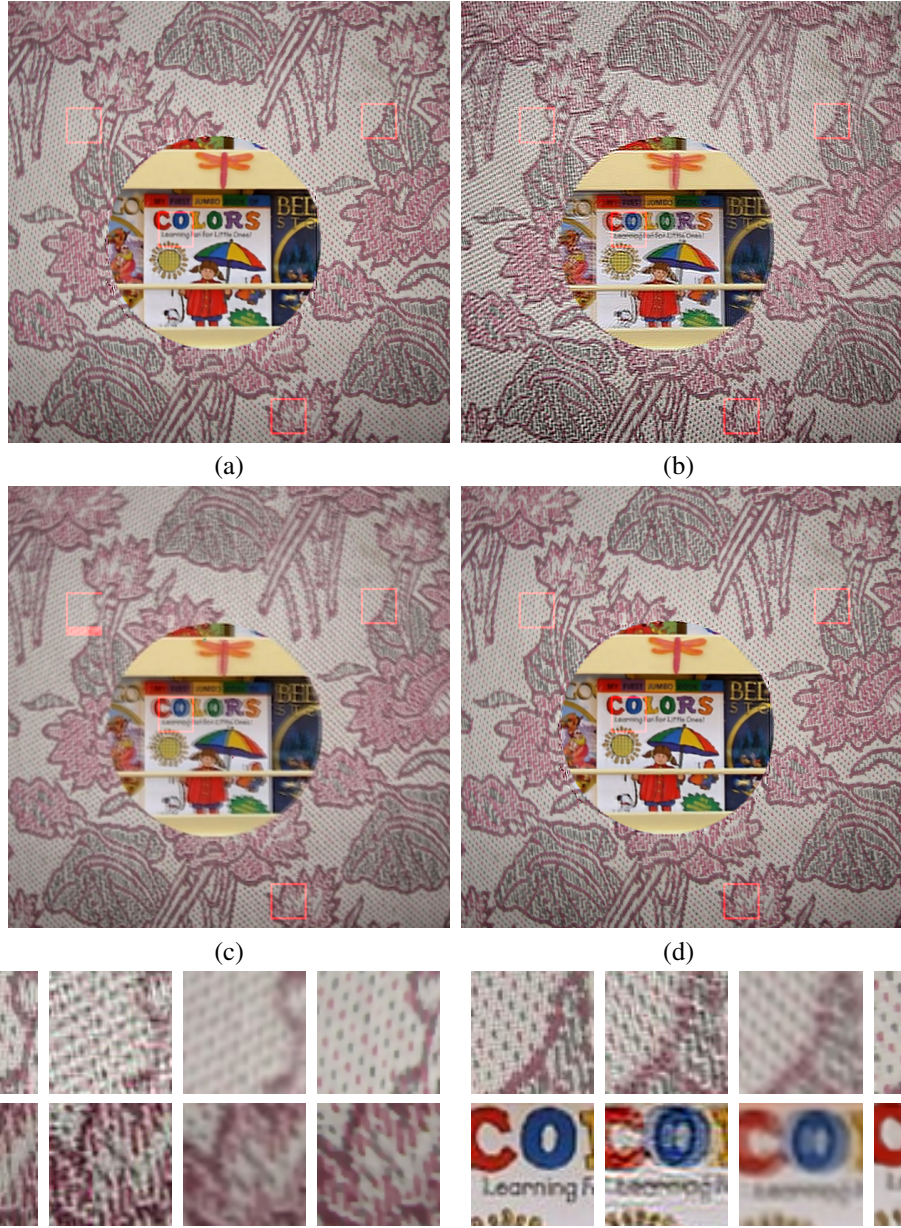


Figure 5. (a) Original image. Estimated latent image from the method of (b) [10], (c) [23], and (d) the proposed approach. Rows 3 and 4: Zoomed-in patches cropped from the original image, output of [10], output of [23], and the estimate from proposed method (in each of the four sets of patches).



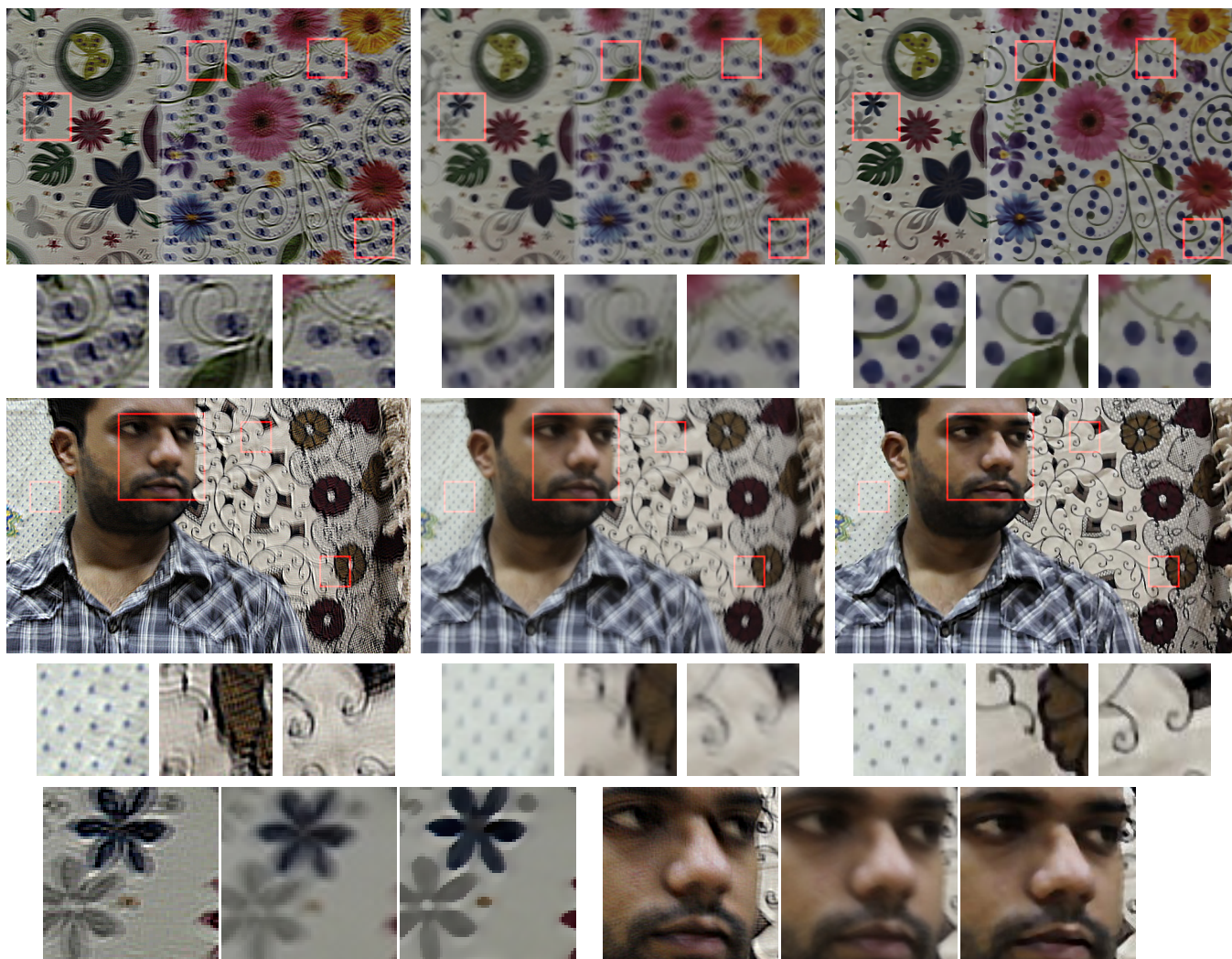


Figure 6. Rows 1 to 4, first column: results from [10], second column: results from [23], third column: results from the proposed method. Row 5: zoomed-in patches from the estimate of [10], [23], and the proposed method (in each of the two sets of patches).